

独立反谐振纤芯低损耗光子带隙光纤

高福宇^{1*}, 徐小斌¹, 宋凝芳¹, 李伟², 朱云浩¹, 刘嘉琪¹, 梁田田¹

¹北京航空航天大学仪器科学与光电工程学院, 北京 100191;

²锐光信通科技有限公司, 湖北 武汉 430074

摘要 光子带隙光纤具有弯曲损耗小、对环境变化不敏感等优点, 是极端应用条件下高稳定光纤陀螺的理想光纤。但光子带隙光纤的传输损耗大, 缺乏适用于光纤陀螺的低损耗、小模场光子带隙光纤。提出了独立反谐振纤芯光纤构型, 将纤芯与包层进行空间隔离, 利用纤芯壁反谐振效应抑制基模与表面模的耦合, 利用反谐振与光子带隙双重效应将光限制在纤芯中传输, 从而实现了光子带隙光纤小模场、低损耗的特性。理论分析结果表明, 所提出的光纤构型可将模场直径为 $\sim 8 \mu\text{m}$ 的光子带隙光纤的损耗降低至 $< 3.5 \text{ dB/km}$ 。采用两步法制备的光纤基本复现了设计结构, 但占空比与设计值存在偏差, 导致带隙偏移, 实验测得所制备光纤的最小损耗为 $\sim 25 \text{ dB/km}$ @1200 nm。

关键词 光纤光学; 光纤设计; 光子带隙光纤; 低损耗; 小模场直径

中图分类号 TN253

文献标志码 A

DOI: 10.3788/CJL202249.1906002

1 引言

光子带隙光纤(PBF)基于蜂窝状微米级空气孔结构形成了光子晶体包层, 产生的光子带隙效应将光波限制在中空纤芯中传输。Russell^[1]提出了光子晶体光纤的概念, 其传输原理与传统光纤不同, 光可以在空气中稳定传输, 由于空气性质比石英玻璃更稳定, 因此光子晶体光纤具有环境稳定性。光子晶体光纤一直是新型光纤领域的研究热点, 目前已实现的空芯光纤主要分为光子带隙光纤与反谐振光纤(ARF)。随着光子带隙光纤制备工艺的不断进步, 光纤损耗逐步降低, 19-芯光子带隙光纤的损耗降低至 1.7 dB/km ^[2]。但增大纤芯直径的方式也使得光纤的抗弯曲性能明显下降, 当 19-芯光子带隙光纤在 $3.5 \mu\text{m}$ 波段弯曲成直径为 5 cm 的圆时, 损耗增加 0.25 dB ^[3]。随着光子带隙光纤理论与制备技术的发展, 研究者设计了空芯反谐振光纤。嵌套管型无结点反谐振光纤的损耗降低至 0.28 dB/km ^[4]。2022 年, 嵌套型无结点反谐振光纤的损耗已降至 0.17 dB/km 。受传输原理的限制, 与光子带隙光纤相比, 反谐振光纤的模场直径和弯曲损耗更大, 在 1550 nm 传输波段, 当低损耗嵌套型反谐振空芯光纤的弯曲直径为 4 cm 时, 附加损耗约为 0.2 dB/m ^[4]。与传统光纤相比, 光子带隙光纤具有结构设计灵活性高、环境敏感性低^[5]、非线性极低^[6]等优点, 光子带隙光纤陀螺(PBFOG)成为光子带隙光纤最有前景的应用之一。采用光子带隙光纤作为陀螺的敏

感环光纤, 可从根本上解决辐射^[7]等环境因素对光纤陀螺的影响^[8-9]。

增大纤芯直径可以减少基模与纤芯壁的重叠, 是降低光纤散射损耗的有效方法。因此, 与小模场的 7 芯 PBF 相比, 19 芯和 37 芯大纤芯直径 PBF 具备更低的损耗^[10-12]。然而, 大模场易导致光纤的抗弯曲性能下降, 产生更多的高阶模式^[12], 并且增加了光纤与光学器件之间低损耗耦合的难度。研究人员针对 7 芯 PBF 开展了表面模分析^[13]、结构设计^[14]以及熔接耦合技术^[15]研究, 小芯径、低损耗空芯光纤在保证光纤对环境不敏感的同时, 兼顾了与传统光学器件耦合的性能, 更适用于光纤陀螺等传感器^[16]。

本文在传统光子带隙光纤的基础上, 设计并制备了独立反谐振纤芯光子带隙光纤(IAC-PBF), 这种新型空芯光纤的包层结构与传统的 7 芯 PBF 相同, 但纤芯由一个独立的六边形反谐振层构成, 在小模场的前提下兼顾了 PBF 抗弯曲和 ARF 低损耗的优点。仿真结果表明, 该光纤具有 $\sim 3.5 \text{ dB/km}$ 的低损耗, 且模场直径为 $\sim 8 \mu\text{m}$, 与传统光纤、器件的模场相匹配, 同时兼具抗弯曲性能, 是干涉式高精度光纤陀螺的理想光纤。

2 光纤设计与仿真

2.1 反谐振层光纤建模

光子带隙光纤的损耗主要来源于散射损耗。改变纤芯厚度可产生反谐振效应, 从而降低纤芯壁光能量, 可有效降低散射损耗^[2]。光被限制在空气纤芯中传

收稿日期: 2022-05-18; 修回日期: 2022-05-30; 录用日期: 2022-07-06

基金项目: 国家自然科学基金(61935002)、国防科技重点实验室基金(2021-JCJQ-LB-070-23)

通信作者: *gaofuyu@buaa.edu.cn

输,当波长恰好满足纤芯壁中传输的谐振条件时,光容易耦合到纤芯壁中,引起光纤损耗增加。将纤芯壁近似为对称的三层平板波导,其中传输波长 λ 与反谐振层厚度 t 之间的关系为

$$m \frac{\lambda}{2} = t \cdot \sqrt{n_{\text{silica}}^2 - 1}, \quad (1)$$

式中: m 为正整数; n_{silica} 为石英玻璃的折射率。因此,设置纤芯壁厚度,使传输光在纤芯壁中的谐振条件不被满足,即可有效降低光纤损耗。

独立反谐振纤芯结构的光子带隙光纤的微孔结构如图 1(a)所示,其包层结构与普通的光子带隙光纤相同,仍然是基于周期排布的六边形空气孔形成光子晶体结构,并产生光子带隙效应,阻止光从包层中泄漏。纤芯区域的放大图像如图 1(b)所示,其中 R 是纤芯半径, t 是纤芯壁厚度,即独立反谐振层厚度, Λ 、 d 和 d_c

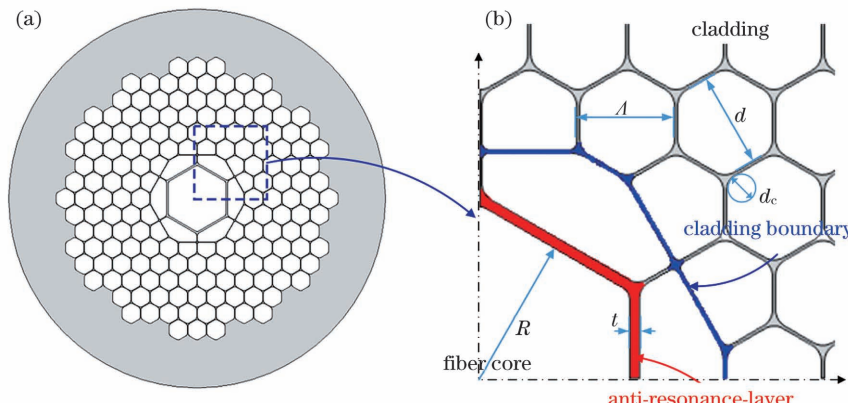


图 1 独立反谐振纤芯光子带隙光纤结构。(a)IAC-PBF 的空芯微孔结构;(b)IAC-PBF 的纤芯结构

Fig. 1 Isolated anti-resonant core photonic band-gap fiber structure. (a) Hollow core microporous structure of IAC-PBF; (b) core structure of IAC-PBF

2.2 参数仿真

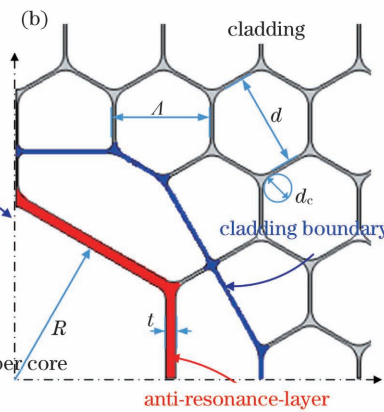
光纤损耗的仿真采用 F 参数法:

$$F = \left(\frac{\epsilon_0}{\mu_0} \right)^{1/2} \times \frac{\oint_{\text{hole-perimeter}} |\mathbf{E}|^2 dl}{\int_{\text{cross-section}} \mathbf{E} \times \mathbf{H}^* \cdot \mathbf{z} dA}, \quad (2)$$

式中: $\epsilon_0 = 8.8542 \times 10^{-12} \text{ C}^2/(\text{N} \cdot \text{m}^2)$ 为真空介电常数(电容率); $\mu_0 = 4\pi \times 10^{-12} \text{ N}^2 \cdot \text{s}^2/\text{C}^2$ 为真空磁导率; \mathbf{E} 为光波的电场强度; l 为微孔边界长度; \mathbf{H} 为光波的磁场强度; $*$ 为取共轭; \mathbf{z} 为截面单位法向量; A 为横截面面积。此参数 F 表征了石英玻璃壁与空气界面处的光能量与传输总能量的比值。

根据仿真分析结果可知,当 $0.4 \mu\text{m} \leq t \leq 0.6 \mu\text{m}$ 时,光纤损耗在 1550 nm 波段均达到较为理想的状态,与空芯反谐振光纤的纤芯壁厚度相当,而此时为了保证其模场直径与传统光纤相近并减小应用过程中与传统光纤、器件的耦合损耗,设计纤芯直径为 $\sim 13 \mu\text{m}$,模场直径(MFD)为 $\sim 8 \mu\text{m}$,其模场分布如图 2(b)所示。当纤芯反谐振壁过薄时,其对传输光的限制能力降低,且纤芯壁的表面模增多,纤芯中的光可

分别为空气孔周期、空气孔内径和倒角直径。根据前期研究^[17],在 1550 nm 传输波段处所选取的包层微孔结构参数为 $\Lambda = 4 \mu\text{m}$, $d/\Lambda = 0.97$, $d_c/d = 0.4$ 。模场直径与芯径有关,因此将 R 设为 $\sim 6.5 \mu\text{m}$,此时模场直径为 $\sim 8 \mu\text{m}$,与常规单模光纤及器件相匹配。不同之处在于,此光纤的纤芯不再是由 12 个空气孔围成,而是由单独的毛细管拉制而成,纤芯与包层被 6 个相同且较大的六边形隔断。纤芯与包层被空间隔离,这使得纤芯模式与包层模及光子晶体截断处的表面模的耦合大幅减弱,图 1(b)为反谐振层(anti-resonance-layer)形成的纤芯结构。表面模多出现在微孔结构的边界(cladding boundary)处,尤其是周期性结构的截断面,通过边界石英壁厚度的调节可改变表面模折射率,因此反谐振纤芯最主要的参数是纤芯壁厚度。



直接或通过与表面模耦合的方式泄漏,光纤损耗增大。而当纤芯反谐振壁厚度增加并接近谐振厚度时,反谐振效应减弱,光纤损耗增大。因此,独立反谐振纤芯结构的光子带隙光纤的纤芯壁厚为 $\sim 0.4 \mu\text{m}$ 时可达到损耗最低值,目前的光子带隙光纤拉制工艺可将损耗降低至 $\sim 3.5 \text{ dB/km}$ 。

IAC-PBF 的损耗谱不平坦,在某些波长处存在损耗突增的情况,这是由于此结构虽然降低了纤芯模式与包层模式的耦合,纤芯壁中的表面模仍然存在。光纤中存在的模式如图 3 所示,其中图 3(a)为纤芯中的基模(LP_{01} 模式),图 3(b)为包层壁的表面模,图 3(c)~(e)为纤芯壁的表面模,图 3(f)为纤芯中的高阶模。包层壁的表面模与纤芯模式几乎不发生模式耦合,因此可将包层周期结构截断处的表面模忽略,最大程度地保持理想光子晶体的包层结构对传输光的限制作用。

为了明确光纤损耗的变化原因,本文对光纤基模与纤芯壁表面模的耦合特性进行了仿真分析。独立反谐振纤芯光子带隙光纤在不同纤芯厚度下的模式耦合

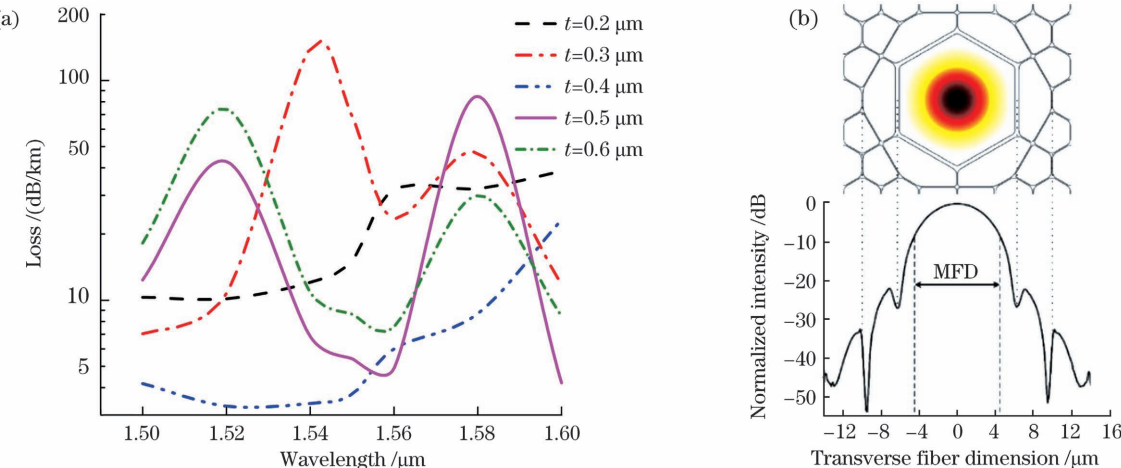


图 2 独立反谐振纤芯光子带隙光纤的损耗及模场仿真结果。(a)不同纤芯壁厚度下的损耗;(b)模场直径

Fig. 2 Loss and mode field simulation results of IAC-PBF. (a) Losses under different core wall thicknesses; (b) mode field diameter

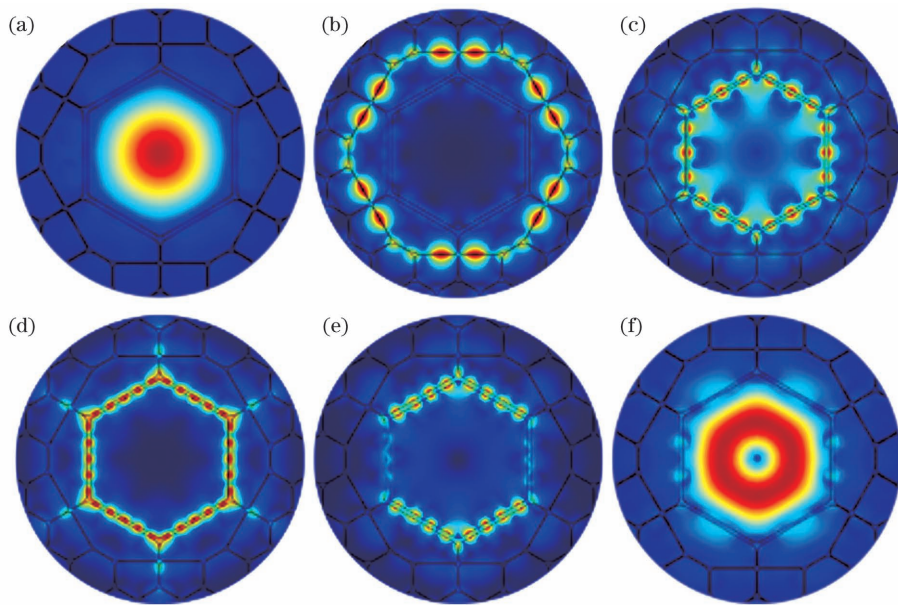


图 3 独立反谐振纤芯光子带隙光纤的模式。(a)基模;(b)包层壁的表面模;(c)(d)(e)纤芯壁的表面模;(f)纤芯中的高阶模

Fig. 3 Modes of IAC-PBF. (a) Fundamental mode; (b) surface mode in cladding wall; (c)(d)(e) surface modes in fiber core wall; (f) high-order mode in fiber core

仿真结果如图 4 所示,模式耦合的发生需要满足两个基本条件:一是两模式存在空间交叠,二是相位匹配。通过仿真分析可见:当纤芯壁较薄时,基模与纤芯壁的表面模耦合;当纤芯壁的厚度大于 $0.4\text{ }\mu\text{m}$ 时,纤芯壁的表面模与高阶模耦合,且模式折射率远离基模,因此基模与表面模及高阶模式不耦合。当 $t=0.4\text{ }\mu\text{m}$ 时,各模式下的损耗计算结果如表 1 所示,可见此结构的光子晶体光纤的理论损耗可以降低到 $\sim 3\text{ dB/km}$,而高阶模式损耗比基模损耗大 10 dB/km 。因此,该结构的光纤能够保证基模低损耗传输,同时增大了高阶模式损耗,使得光纤进行长距离传输时,能够保持一定的单模传输特性。

本文对 IAC-PBF 的弯曲损耗进行了仿真分析,其中光纤损耗包含光纤在弯曲条件下的散射损耗与限制损耗,理论分析结果如图 5 所示。由于纤芯为轴对称结构,仿真选取了图 5 插图所示的两个典型弯曲方向,分别为 0° 位置和 30° 位置。由结果可知,两角度位置处的弯曲损耗特性几乎一致。模场在弯曲作用下偏离中心位置,光纤在小弯曲半径时的损耗较大,且随着弯曲半径的增加而快速减小,在弯曲半径为 $\sim 13\text{ mm}$ 时损耗最低,之后随弯曲半径的增加,损耗小幅增加。总体而言,光纤的弯曲损耗变化在 $\sim 0.3\text{ dB/km}$ 以内,光子带隙光纤优良的弯曲特性得到保持。

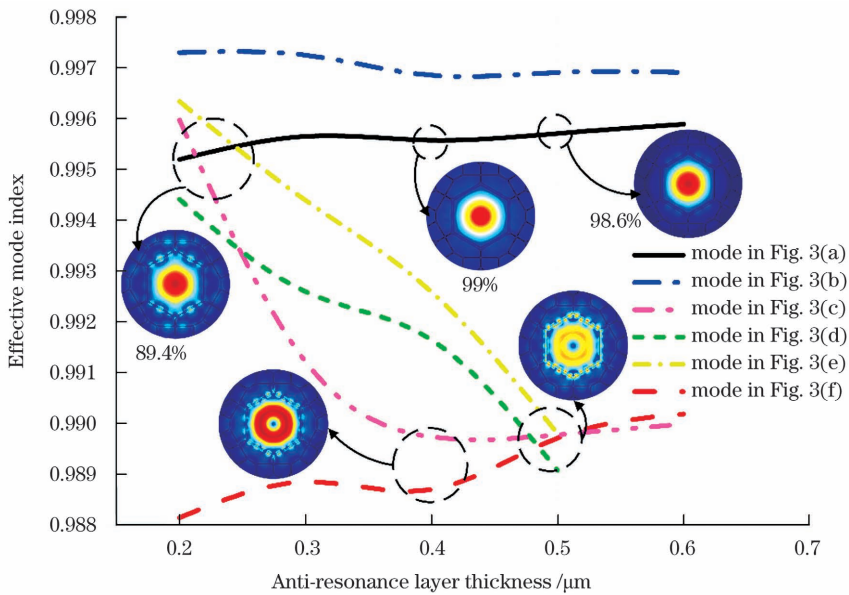


图 4 独立反谐振纤芯光子带隙光纤在不同纤芯厚度下的模式耦合
Fig. 4 Mode coupling of IAC-PBF under different fiber core thicknesses

表 1 独立反谐振纤芯光子带隙光纤中各模式的损耗

Table 1 Loss of each mode in IAC-PBF

Mode	Loss /(dB/km)	Mode	Loss /(dB/km)
Mode in Fig. 3(a)	3.05	Mode in Fig. 3(d)	599.10
Mode in Fig. 3(b)	570.30	Mode in Fig. 3(e)	555.90
Mode in Fig. 3(c)	602.90	Mode in Fig. 3(f)	13.40

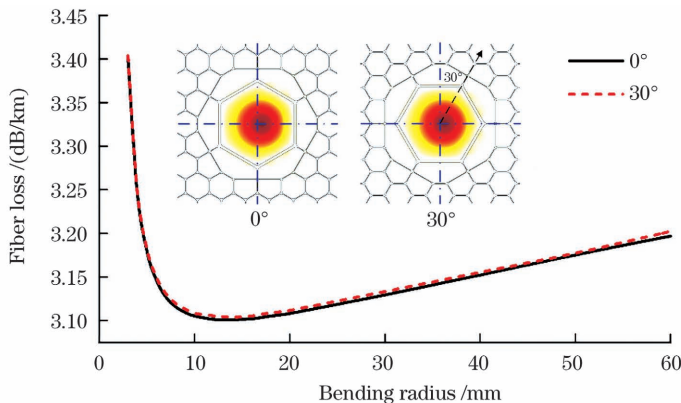


图 5 独立反谐振纤芯光子带隙光纤的弯曲损耗
Fig. 5 Bending loss of IAC-PBF

3 IAC-PBF 的制备与测试

独立反谐振纤芯光子带隙光纤仍可采用传统光子带隙光纤的堆积-拉制法制备。将拉制的石英玻璃毛细管堆积为与光纤结构相近的结构，并插入到合适内径的玻璃管中制备预制棒。经过第一步，拉制形成具备类似光纤结构的中间体，此过程实现了毛细管的定位黏接，并采用低气压去除毛细管之间的缝隙，横截面结构如图 6(a)所示，中间体直径为 3~5 mm。将中间体插入外套管中进行第二步拉制，通过分区气压控制实现了微孔尺寸的精确控制，独立反谐振纤芯光子带隙光纤的结构如图 6(b)所示。

实际制备的光纤微孔尺寸小于理论值，为了明确光纤结构整体的复现程度，将理论最优参数下的光纤等比缩小，两者结构的对比如图 7 所示，其中理论光纤构型整体直径等比缩小为理想光纤结构的 3/4，可见光纤整体结构与设计的理论构型基本一致，包层结构得到了完整的复现，但空气孔尺寸缩小。实际纤芯尺寸比设计结构小，实际纤芯直径仅为~8.1 μm(理论设计值为 13 μm)，纤芯壁厚度为~0.18 μm(理论设计值为 0.4 μm)。光纤中空气孔尺寸的缩小将导致光子带隙向短波长方向偏移，过小的纤芯会导致光纤损耗增加，过薄的纤芯壁不仅不利于实现反谐振效应，还会引入较多的表面模。

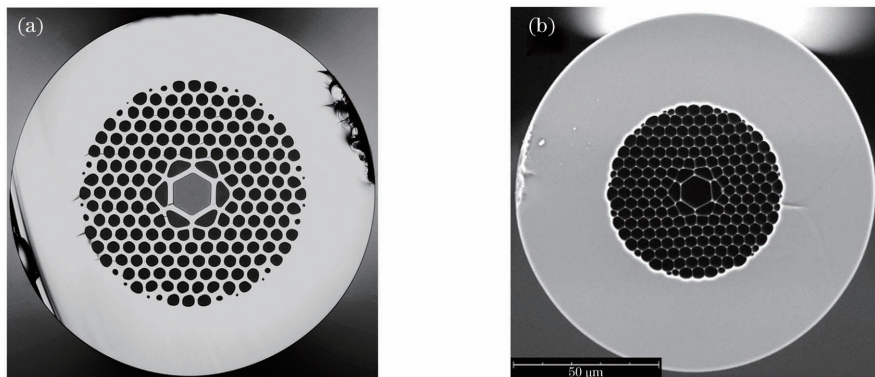


图 6 IAC-PBF 中间体与带隙光纤的结构图。(a)中间体;(b)带隙光纤

Fig. 6 Structural diagrams of IAC-PBF cane and band-gap fiber . (a) Fiber cane; (b) band-gap fiber

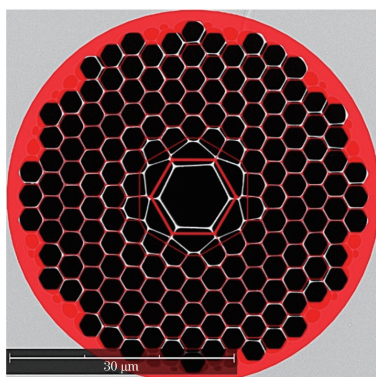


图 7 实际光纤(小纤芯图像)与理论光纤(大纤芯图像)的对比

Fig. 7 Comparison between actual fiber (small core image) and theoretical fiber (large core image)

采用截断法测试的 IAC-PBF 损耗谱如图 8 所示, 可见此结构的 IAC-PBF 的带隙移动到 1200 nm 处, 最低损耗约为 25 dB/km, 纤芯壁过薄导致光纤中存在较为严重的表面模。利用实际光纤结构的测试结果, 逆向建立 IAC-PBF 仿真模型, 计算光纤内部的模场分布。在传输波段~1200 nm 处, 光纤中的模式基本被限制在纤芯中, 纤芯壁的表面模较少, 当传输波段在 1400 nm 处时, 光纤损耗达到 200 dB/km, 仿真可见光

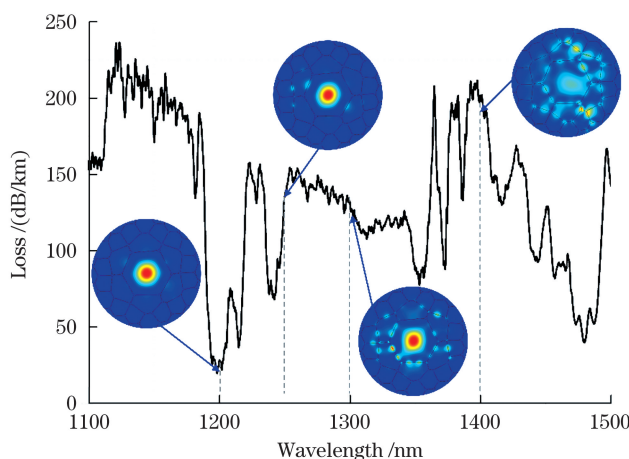


图 8 IAC-PBF 的损耗谱测试结果与模场仿真对比

Fig. 8 Measured loss spectrum and simulated mode field of IAC-PBF

纤中的基模与表面模式发生耦合, 在带隙内存在较多的表面模。根据文献[2]中的研究结果可知, 光子带隙光纤的散射损耗与波长的立方成反比, 可推测在此纤芯结构尚不完美的条件下, 若光子带隙位置在 1550 nm 处, 光纤损耗为~11.6 dB/km, 验证了所设计的 IAC-PBF 具备小模场、低损耗的优点。

4 结 论

光子带隙光纤与反谐振光纤相比, 虽然损耗大, 但具备小模场、抗弯曲的特性, 是高稳定光纤陀螺的理想材料。光子带隙光纤的损耗主要源于纤芯结构引起的基模与纤芯壁表面模的耦合, 以及粗糙微孔内壁导致的大散射损耗。对纤芯结构进行了几何参数关联的仿真分析, 设计了独立反谐振纤芯光子带隙光纤新构型。此构型将纤芯与包层进行了空间隔离, 大幅降低了基模与包层表面模的耦合; 采用反谐振纤芯增强了对纤芯中基模的限制, 压缩了基模模场, 降低了散射损耗。此外, 独立反谐振纤芯结构是由独立的毛细管堆积而成的, 独立毛细管构成的纤芯厚度易于控制, 相比传统光子带隙光纤, 纤芯壁粗糙度降低, 在相同工艺条件下光纤损耗大幅降低。理论上可实现模场直径为~8 μm、损耗<3.5 dB/km(@1550 nm)的独立反谐振纤芯光子带隙光纤。采用堆积-拉制法制备了光纤样品, 纤芯直径为~8.1 μm 时传输损耗为~25 dB/km(@1200 nm)。

参 考 文 献

- [1] Russell P S J. Optics of Floquet-Bloch waves in dielectric gratings[J]. Applied Physics B, 1986, 39(4): 231-246.
- [2] Mangan B J, Farr L, Langford A, et al. Low loss (1.7 dB/km) hollow core photonic bandgap fiber [C] // Optical Fiber Communication Conference 2004, February 22, 2004, Los Angeles, California, USA. Washington, D. C.: OSA, 2004: PD24.
- [3] Wheeler N V, Heidt A M, Baddela N K, et al. Low-loss and low-bend-sensitivity mid-infrared guidance in a hollow-core-photonic-bandgap fiber[J]. Optics Letters, 2014, 39(2): 295-298.
- [4] Jasion G T, Bradley T D, Harrington K, et al. Hollow core NANF with 0.28 dB/km attenuation in the C and L bands[C] // 2020 Optical Fiber Communications Conference and Exhibition

- (OFC), March 8-12, 2020, San Diego, CA, USA. New York: IEEE Press, 2020.
- [5] Ma P, Song N F, Jin J, et al. Birefringence sensitivity to temperature of polarization maintaining photonic crystal fibers [J]. Optics & Laser Technology, 2012, 44(6): 1829-1833.
- [6] Ouzounov D G, Ahmad F R, Müller D, et al. Generation of megawatt optical solitons in hollow-core photonic band-gap fibers [J]. Science, 2003, 301(5640): 1702-1704.
- [7] Digonnet M, Blin S, Kim H K, et al. Sensitivity and stability of an air-core fibre-optic gyroscope [J]. Measurement Science and Technology, 2007, 18(10): 3089-3097.
- [8] Olanterä L, Sigaud C, Troska J, et al. Gamma irradiation of minimal latency hollow-core photonic bandgap fibres [J]. Journal of Instrumentation, 2013, 8(12): C12010.
- [9] 徐小斌, 王晓阳, 高福宇, 等. 光子晶体光纤陀螺技术及其首次空间试验 [J]. 中国惯性技术学报, 2021, 29(1): 1-7.
- Xu X B, Wang X Y, Gao F Y, et al. Photonic crystal fiber-optic gyroscope technology and its first space experiment [J]. Journal of Chinese Inertial Technology, 2021, 29(1): 1-7.
- [10] Amezcua Correa R, Broderick N G R, Petrovich M N, et al. Design of 7 and 19 cells core air-guiding photonic crystal fibers for low-loss, wide bandwidth and dispersion controlled operation [J]. Optics Express, 2007, 15(26): 17577-17586.
- [11] Petrovich M N, Baddela N K, Wheeler N V, et al. Development of low loss, wide bandwidth hollow core photonic bandgap fibers [C]// Optical Fiber Communication Conference/National Fiber Optic Engineers Conference 2013, March 17-21, 2013, Anaheim, California. Washington, D.C.: OSA, 2013: OTh1J.3.
- [12] Fokoua E R N. Ultralow loss and wide bandwidth hollow-core photonic bandgap fibres for telecom applications [D]. Southampton: University of Southampton, 2015.
- [13] 游永, 郭慧毅, 李伟, 等. 空芯光子带隙光纤中的表面模共振耦合效应及高温传感特性 [J]. 光学学报, 2021, 41(13): 1306005.
- You Y, Guo H Y, Li W, et al. Surface-mode resonance coupling effect and high-temperature sensing characteristics in hollow-core photonic bandgap fibers [J]. Acta Optica Sinica, 2021, 41(13): 1306005.
- [14] 张亚奇, 刘硕, 白振旭. $2\mu\text{m}$ 波段 7-cell 空芯光子带隙光纤的特性研究 [J]. 光电技术应用, 2021, 36(1): 34-38, 63.
- Zhang Y Q, Liu S, Bai Z X. Research on characteristics of $2\mu\text{m}$ band 7-cell hollow core photonic bandgap fiber [J]. Electro-Optic Technology Application, 2021, 36(1): 34-38, 63.
- [15] 况心怡, 钮月萍, 龚尚庆. 空芯光子带隙光纤与单模光纤的电弧熔接研究 [J]. 激光与光电子学进展, 2020, 57(17): 170601.
- Kuang X Y, Niu Y P, Gong S Q. Arc fusion splicing between hollow-core photonic bandgap fiber and single-mode fiber [J]. Laser & Optoelectronics Progress, 2020, 57(17): 170601.
- [16] Gao F Y, Song N F, Xu X B, et al. Low-loss hollow-core photonic bandgap fiber with isolated anti-resonance layer [J]. Optics Communications, 2019, 441: 208-211.
- [17] Xu X B, Gao F Y, Zhang Z H, et al. An investigation of numerical aperture of air-core photonic bandgap fiber [J]. Science China Technological Sciences, 2015, 58(2): 352-356.

Low-Loss Isolated Anti-Resonant Core Photonic Bandgap Fiber

Gao Fuyu^{1*}, Xu Xiaobin¹, Song Ningfang¹, Li Wei², Zhu Yunhao¹, Liu Jiaqi¹, Liang Tiantian¹

¹ School of Instrumentation and Optoelectronic Engineering, Beihang University, Beijing 100191, China;

² Ruiguang Xintong Technology Co., Ltd., Wuhan 430074, Hubei, China

Abstract

Objective The advantages of photonic bandgap fiber (PBF) in terms of temperature, radiation, magnetic field, and other aspects of environmental adaptability make it an important development direction of fiber optic gyroscope technology. PBF has attracted extensive attention from research institutions worldwide. However, the fiber loss of seven-core PBF which is suitable for fiber-optic gyroscopes is large, and the PBF cannot meet the low-loss application requirements of fiber-optic gyroscopes for fibers.

Methods The PBF loss is mainly caused by the coupling between the fundamental mode and surface modes of the core wall, and the scattering loss caused by the roughness of the inner wall of the fiber core. In this study, an isolated anti-resonant core photonic bandgap fiber (IAC-PBF) is developed, in which the fiber structure can isolate the core from the cladding, thereby the coupling between the fundamental mode and surface mode is suppressed through the anti-resonant effect of the core wall. An IAC-PBF structural model is established and the loss of the fiber is calculated using the F parameter method. The optimized fiber structure is obtained by scanning the structural parameters. The mode characteristics of the fiber and the loss reduction principle are determined by mode coupling analysis, and it is verified that the proposed fiber structure has low theoretical loss. Finally, the fiber is fabricated using the stacking-drawing method. Although the core size is small and the bandgap is offset, the feasibility of low-loss fiber is proved.

Results and Discussions The IAC-PBF structure is proposed in this article (Fig. 1). Its cladding structure is the same as that of 19-cell PBF, and the photonic crystal structure is still formed through the periodic arrangement of hexagonal air holes to generate the photonic bandgap effect to prevent light leakage from the cladding. A hexagonal anti-resonance layer is used to isolate the core and cladding layers spatially. This reduces the mode coupling and scattering loss. The mode field diameter is approximately $8\mu\text{m}$, and the fiber loss is less than 3.5 dB/km , which is achievable with the current fiber fabrication process (Fig. 2). The reason for the increase in loss caused by structural changes is studied based on the relationship between the mode coupling and the structure of the PBF (Fig. 4). The simulation results show that the fundamental mode couples with the surface mode of the core wall when the core wall is thin. When the thickness of the

core wall is greater than $0.4 \mu\text{m}$, the surface mode of the core wall is coupled with the higher-order mode, and the mode refractive index is far from that of the fundamental mode, ensuring the decoupling of the fundamental mode from the surface mode and higher-order mode. For the bending loss, when the bending radius is greater than 4 mm, the bending loss of the IAC-PBF varies within 0.3 dB/km, maintaining the excellent bending characteristics of the PBF (Fig. 5). The IAC-PBF is fabricated using the stacking-drawing method (Fig. 7). The feasibility and loss reduction effect of the proposed fiber structure are verified by fiber testing and theoretical analysis, laying a foundation for the subsequent development of long-distance PBFs with a small mode field and low loss (Fig. 8). Theoretical simulation and experimental results show that IAC-PBF exhibits small fiber loss, a small mode field diameter, and bending resistance.

Conclusions Compared with anti-resonance fiber, the PBF has relatively large loss but a small mode field and bending resistance, making it an ideal fiber for a high-stability fiber-optic gyroscope. In this study, an isolated anti-resonance core photonic bandgap fiber is designed. In this configuration, the core and cladding are spatially isolated, and the coupling between the fundamental and cladding surface modes is significantly reduced. An anti-resonance core is used to enhance the confinement of the fundamental mode, compress the fundamental mode field, and reduce the scattering loss. At the same time, the core structure of the IAC-PBF is formed by a stack of independent capillaries, unlike the traditional bandgap fiber which is formed by the capillary surrounding the fiber core. In the process of drawing, it is easy to control the fiber core thickness and reduce the roughness of the core wall, which can significantly reduce the fiber loss. The theoretical analysis results show that the loss of the PBF with a mode field diameter of approximately $8 \mu\text{m}$ can be reduced to less than 3.5 dB/km. The structure of the fiber is basically reproduced, but the difference in the quartz wall thickness causes a shift in the bandgap. The minimum loss of the fiber is approximately 25 dB/km @ 1200 nm.

Key words fiber optics; fiber design; photonic band-gap fiber; low loss; small mode field diameter